# Relationship of edge localized mode burst times with divertor flux loop signal phase in JET

S. C. Chapman, R. O. Dendy, T. N. Todd, N. W. Watkins, A. J. Webster, F. Calderon, J. Morris, and JET EFDA Contributors

Citation: Physics of Plasmas (1994-present) **21**, 062302 (2014); doi: 10.1063/1.4881474
View online: http://dx.doi.org/10.1063/1.4881474
View Table of Contents: http://scitation.aip.org/content/aip/journal/pop/21/6?ver=pdfcov
Published by the AIP Publishing

# Relationship of edge localized mode burst times with divertor flux loop signal phase in JET

S. C. Chapman,[1,2,a)] R. O. Dendy,[1,3,4] T. N. Todd,[3,4] N. W. Watkins,[1,2,5,6] A. J. Webster,[3,4] F. Calderon,[1] J. Morris,[3,4] and JET EFDA Contributors[4,b)]
[1]*Centre for Fusion, Space and Astrophysics, Department of Physics, University of Warwick, Coventry, United Kingdom*
[2]*Max Planck Institute for the Physics of Complex Systems, Dresden, Germany*
[3]*Euratom/CCFE Fusion Association, Culham Science Centre, Abingdon, Oxfordshire, United Kingdom*
[4]*JET-EFDA, Culham Science Centre, Abingdon, Oxfordshire, United Kingdom*
[5]*Centre for the Analysis of Time Series, London School of Economics, London, United Kingdom*
[6]*Department of Engineering and Innovation, Open University, Milton Keynes, United Kingdom*

(Received 17 April 2014; accepted 20 May 2014; published online 3 June 2014)

A phase relationship is identified between sequential edge localized modes (ELMs) occurrence times in a set of H-mode tokamak plasmas to the voltage measured in full flux azimuthal loops in the divertor region. We focus on plasmas in the Joint European Torus where a steady H-mode is sustained over several seconds, during which ELMs are observed in the Be II emission at the divertor. The ELMs analysed arise from intrinsic ELMing, in that there is no deliberate intent to control the ELMing process by external means. We use ELM timings derived from the Be II signal to perform direct time domain analysis of the full flux loop VLD2 and VLD3 signals, which provide a high cadence global measurement proportional to the voltage induced by changes in poloidal magnetic flux. Specifically, we examine how the time interval between pairs of successive ELMs is linked to the time-evolving phase of the full flux loop signals. Each ELM produces a clear early pulse in the full flux loop signals, whose peak time is used to condition our analysis. The arrival time of the following ELM, relative to this pulse, is found to fall into one of two categories: (i) prompt ELMs, which are directly paced by the initial response seen in the flux loop signals; and (ii) all other ELMs, which occur after the initial response of the full flux loop signals has decayed in amplitude. The times at which ELMs in category (ii) occur, relative to the first ELM of the pair, are clustered at times when the instantaneous phase of the full flux loop signal is close to its value at the time of the first ELM.  [http://dx.doi.org/10.1063/1.4881474]

## I. INTRODUCTION

Edge localized modes (ELMs)[1–5] are intense, short duration relaxation events observed in enhanced confinement (H-mode) regimes in tokamak plasmas. Each ELM releases particles and energy which load the plasma facing components; scaled up to ITER,[6] the largest such loads would be unacceptable and thus ELM prediction, mitigation, and control are central to magnetic confinement fusion research. The peeling-ballooning MHD instability of the plasma edge is believed to underly ELM initiation, and there is local imaging of precursor plasma fingers.[7] However, there exists no comprehensive understanding of the ELMing process from start to finish, in terms of self-consistent nonlinear plasma physics. Characterization of the dynamics of ELMing processes via their quantitative statistical signatures is relatively novel.[8–10] It may also be informative to quantify, as here, the statistical signatures of correlation between ELMs and signals that capture global plasma dynamics.

In this paper, we perform direct time domain analysis of ELM events in relation to high cadence signals from a system scale diagnostic, the full flux loops in the divertor region in JET. These full flux loop VLD2 and VLD3 signals are proportional to the voltage induced by changes in poloidal magnetic flux. We compare the full flux loop signals with simultaneous Be II emission data which are conventionally used to identify ELM events. We focus on a sequence of JET plasmas that have a steady flat top for $\sim 5\,s$ and which all exhibit intrinsic ELMing in that there is no deliberate intent to control the ELMing process by external means. The noise level in the Be II signal is such that here it is used just to determine the ELM occurrence times. The full flux loop signals show a clear, characteristic large amplitude oscillatory response to each ELM that is identified in the Be II data. The characteristic oscillation timescale of these strongly damped oscillations is $\sim 0.01\,s$. In this data, we identify a class of prompt ELMs with occurrence times that all coincide with the first, large amplitude cycle of this response signal. On longer timescales, the flux loop signal amplitudes decay but still have sufficiently large signal dynamic range, compared to the noise, to allow the time evolving instantaneous phase to be determined on timescales between one ELM and the next. We find a correlation between this full flux loop

a)Electronic mail: S.C.Chapman@warwick.ac.uk
b)All the members of the JET-EFDA collaboration appear in the appendix of F. Romanelli *et al.*, *Proceedings of the 24th IAEA Fusion Energy Conference 2012, San Diego, CA, USA* (International Atomic Energy Agency, Vienna, 2012).

 

instantaneous phase, and ELM occurrence time, for all the non-prompt ELMs in these plasmas. ELMs are more likely to occur when the instantaneous phase of these signals is close to the value at the time of the previous ELM.

## II. TIME SIGNATURES OF PAIRS OF SUCCESSIVE ELMs

We analysed a sequence of JET plasmas, each with flat-top H-mode duration of $\sim 5\,s$. These all exhibit intrinsic ELMing in that there is no attempt to precipitate ELMs; the only externally applied time varying fields are those produced by the control system. The parameters of each plasma are given in Table I, where the last column indicates the time interval over which we perform the data analysis reported here. ELM occurrence times are inferred from the Be II signal, which we will compare with measurements of the inductive voltage in the full flux loops VLD2 and VLD3. These circle the JET tokamak toroidally at a location just below and outside the divertor coils, see, e.g., Fig. 2 of Ref. 11. The signal voltage is induced by changes in poloidal magnetic flux through the surface encompassed by the loops.

We determine the ELM occurrence times $t_N$ by identifying the peak of the Be II signal within each ELM using a method similar to Refs. 10 and 12. We first calculate the 300 point running mean of the Be II signal excluding outliers, which are defined as lying beyond 6 standard deviations. We then consider the signal to contain an ELM only where it exceeds this running mean by 3 standard deviations. To ensure that the largest peak is selected in regions where there are multiple local maxima, the ELM occurrence time is taken to be that of the peak which is the maximum within a 50 data point window. We have verified that this selects one maximum per ELM event with $\sim 98\%$ effectiveness in these datasets. From the occurrence times $t_N$ of these peaks, the time intervals between successive ELMs $\Delta t_N = t_N - t_{N-1}$ are found. These are plotted in Figure 1. The lower panel plots the inter-ELM time intervals versus the value of the peak Be II signal at that ELM occurrence time $t_N$ for all the ELMs in all the plasmas considered here. Colour is used to differentiate between ELMs from different JET plasmas, each plasma being represented by a single colour. The upper panel plots a histogram of the inter-ELM time intervals and its normal kernel density estimate with a bandwidth of $0.001\,s$. For all these plasmas, there is a lower cutoff at $\Delta t \sim 0.01$, and there are vertical gaps at time intervals where ELMs occur less often (compare Ref. 10). There is a group of prompt ELMs

TABLE I. Parameters for the JET plasmas analysed here.

| Shot | $I_p$ (*MA*) | $B_T$ (*T*) | *NBI* (*MW*) | *D* | Flat top (s) |
|---|---|---|---|---|---|
| 83769 | 2 | 2 | 12 | 1.2 | 48.5 – 53.8 |
| 83770 | 2 | 2 | 12 | 1.2 | 49.0 – 53.7 |
| 83771 | 2 | 2 | 12 | 1.2 | 48.5 – 53.8 |
| 83772 | 2 | 2 | 12 | 1.2 | 48.5 – 53.8 |
| 83773 | 2 | 2 | 12 | 1.2 | 48.5 – 53.8 |
| 83774 | 2 | 2 | 12 | 1.2 | 48.5 – 53.9 |
| 83775 | 2 | 2 | 12 | 1.2 | 48.5 – 53.8 |

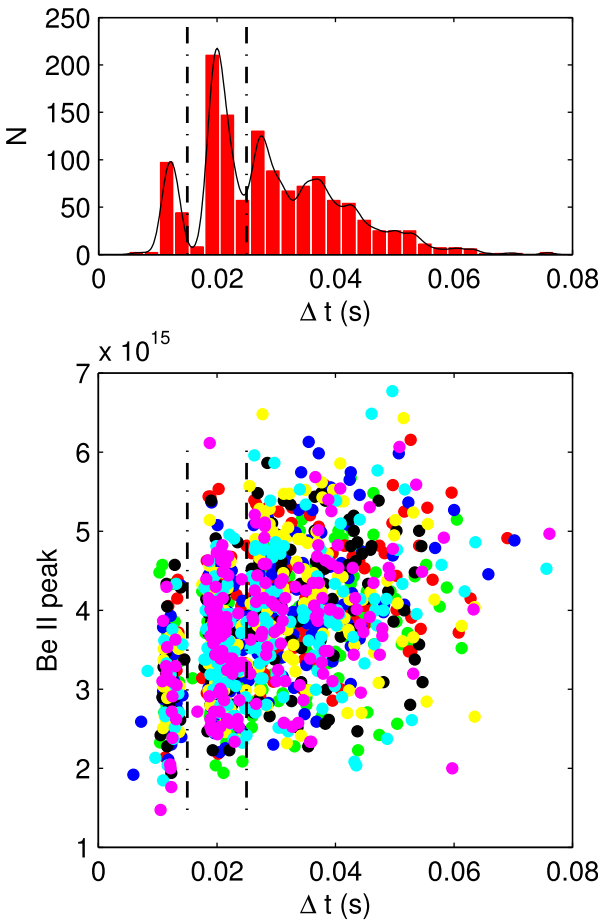


FIG. 1. Lower panel: Peak amplitude of Be II signal for each ELM plotted versus the time interval between one ELM and the next $\Delta t_N$ for the JET plasmas listed in Table I. Upper panel: histogram of these $\Delta t_N$ (red) and kernel density estimate of the histogram (black). Dashed black vertical lines indicate the time intervals $\Delta t = 0.015, 0.025$ s.

which are clustered approximately within $0.01 < \Delta t < 0.015$, and there is a second bunch within $0.015 < \Delta t < 0.025$. For longer $\Delta t$ clear gaps cannot be seen in this size of statistical sample. There is a trend, with a large amount of scatter, for longer inter-ELM time intervals to correspond to larger peak Be II. In particular, the prompt ELMs tend to have smaller peak Be II.

Large ensemble statistical studies across many JET plasmas have revealed[13] that some inter-ELM time intervals are more likely than others. In the single plasmas discussed here, the number of ELMs per plasma ($\sim 100$) is too few to reveal such detail. We find no statistical pattern between the length of one inter-ELM interval and the next.

Figure 1 shows that the empirical probability distribution of time intervals between one ELM and the next has structure. ELMs do not simply arrive at random times, nor are they periodic. We now show that this structure can be identified with features in the full flux loop signals. Signal traces for representative pairs of successive ELMs are shown in Figure 2. In order to compare the full flux loop and Be II signals directly, we first normalize their amplitudes (here and throughout) by dividing by a multiple (10 for Be II, 2 for the VLD2 and 3) of their respective means over the flat-top H-mode duration. The sign convention of the VLD2 and

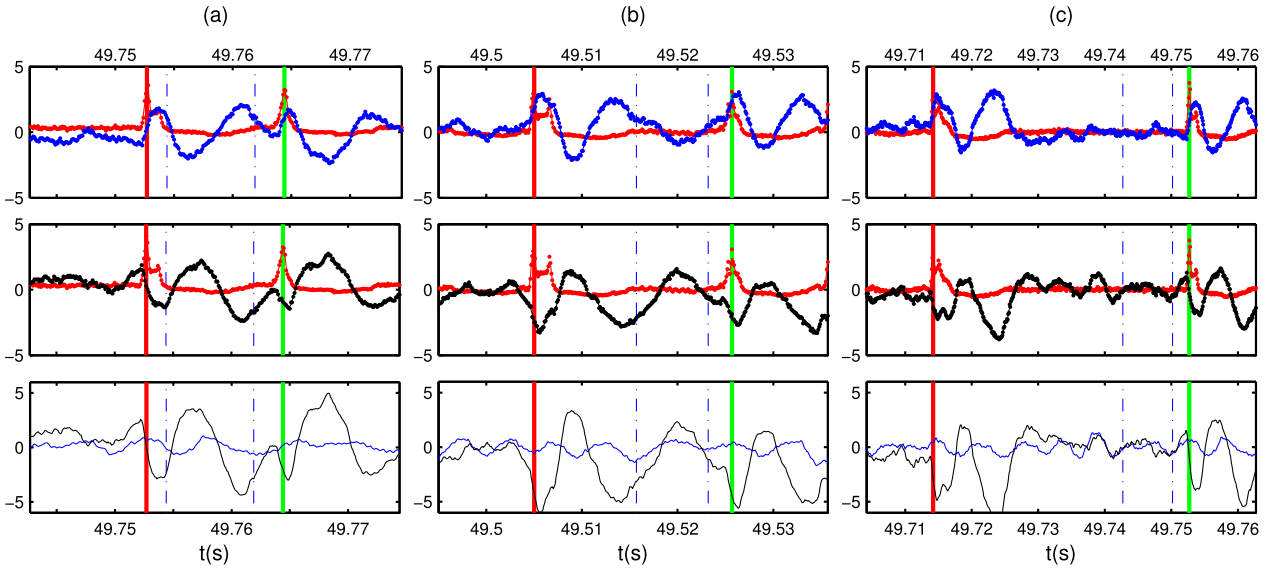


FIG. 2. Time traces for pairs of successive ELMs. Panels (a) are where the second ELM is prompt, it occurs within $0.01 < \Delta t < 0.015$ of the preceding ELM, and within the time when a large amplitude response is seen in the VLD2 and VLD3 traces. Non-prompt ELMs are shown in panels (b) where the second ELM occurs within $0.015 < \Delta t < 0.025$ of the preceding ELM and after the first cycle of the large amplitude response seen in the VLD 2 and VLD3 and panels (c) where the second ELM occurs after $\Delta t > 0.025$ when the large amplitude response in the VLD2 and VLD3 has decayed. Upper panels: time traces of Be II intensity (red), with VLD3 (blue, upper panel) and VLD2 (black, centre panel). The sign convention used here for the VLD2 and VLD3 is such that they have opposite polarity. Data points are plotted as circles and lines are 3 point smoothed. The ELM occurrence times are indicated by vertical red and green lines. Lower panel: difference (black) and sum (blue) of VLD2 and 3. In each panel, amplitudes are: (i) normalized to a long timescale average; (ii) zeroed to the average value just before the second ELM, calculated over the interval denoted by the pair of vertical dot-dash blue lines.

VLD3 signals in these plots is chosen such that they have opposite polarity. The baseline signal value (its mean) varies significantly from one ELM to the next; we therefore choose a single time interval $T_A = [t_N - 0.01, t_N - 0.025]$, relative to each ELM occurrence time $t_N$, within which we calculate both signal means. This time interval is indicated on Figure 2 by the vertical dashed-dotted blue lines. We then subtract this single mean value from the signal which is then plotted in each panel.

The figure shows examples of prompt (a) and non-prompt (b),(c) ELMs. Following each ELM, the figures show a characteristic large amplitude oscillatory response in both of the full flux loop signals, and in their difference, the first cycle of which is on a timescale of ∼0.01 s. The second ELM shown in Figure 2(a) occurs just after the first cycle of this full flux loop response to the first ELM. For this pair of ELMs, the inter-ELM time interval is within the vertical bunch clustered within $0.01 < \Delta t < 0.015$ in Figure 1. Examples of ELMs separated by longer inter-ELM time intervals are shown in Figures 2(b) and 2(c). The inter-ELM time interval lies within the bunch clustered within $0.015 < \Delta t < 0.025$ in Figure 2(b) and is at $\Delta t > 0.025$ in Figure 2(c). We see that the amplitudes of the VLD2 and 3 signals have time to decay over these longer inter-ELM time intervals.

In Figures 3 and 4 we plot the occurrence times of all the pairs of successive ELMs in JET plasma 83770, superimposed on time traces of the corresponding VLD3 signal. To make a systematic comparison, we need to specify a zero time $t_0$ from which to plot the full flux loop signal following the ELM. We could simply choose $t_0 = t_{ELM1}$, the time of the first ELM as determined from the Be II signal. However, the characteristic initial large amplitude oscillatory response to an ELM, which is seen in both the full flux loop signals, provides a better zero time $t_0$. In particular, the times of the extrema of the initial large amplitude response of the full flux loop to an ELM are well defined, and can be determined to a precision of three data points. The Be II signal has a rise time to its peak of ∼10 data points and thus it only determines the ELM occurrence time to this precision. Both full flux loop and Be II signals are at similar cadence. In Figures 3 and 4, we overplot the VLD3 traces as a function of time from $t_0$, that is, versus $t - t_0$. Each trace is thus shifted in time, such that $t - t_0 = 0$ is at the first minimum in the VLD3 signal following the first ELM. We also shift these signals in amplitude such that the traces all pass through zero at $t = t_0$. The occurrence times of the first (red) and second (green) ELMs are also shown. In Figure 3, we plot VLD3 signals and occurrence times for all 154 ELMs. There is

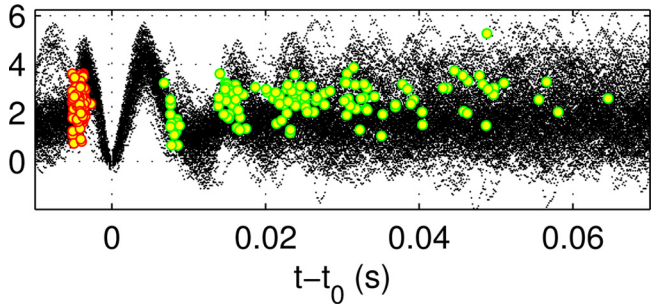


FIG. 3. ELM occurrence times for all ELMs in the ∼5 *s* flat-top of JET plasma 83770 superimposed on the VLD3 signal. The panel plots VLD3 signals (black dotted lines) normalized as in Figure 2. ELM occurrence times are marked on each VLD3 trace with red circles (first ELM) and green circles (second ELM), these symbols/colours will be used in all subsequent plots. These are plotted versus time $t - t_0$, where $t_0$ is at the first minimum in the VLD3 signal following the first ELM. Amplitude is shifted such that the traces pass through zero at $t = t_0$.

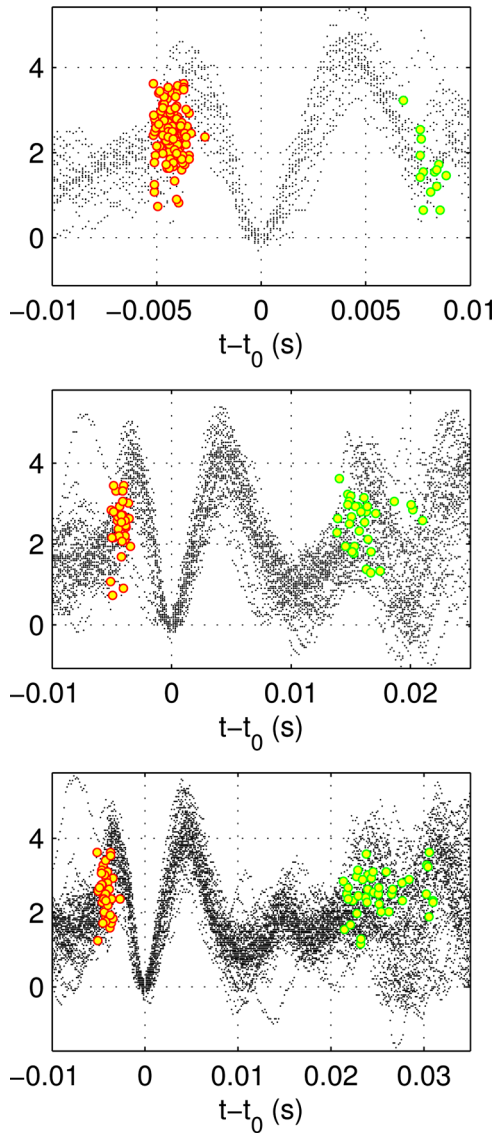


FIG. 4. ELM occurrence times in the ~5 *s* flat-top of JET plasma 83770 superimposed on VLD3 traces, for which the inter-ELM time intervals are in the range: (top) $\Delta t < 0.015$; (centre) $0.015 < \Delta t < 0.025$; (bottom) $0.025 < \Delta t < 0.035$. Each panel is in the same format as Figure 3.

always a clear characteristic response in the VLD3 to the first ELM. Figure 3 suggests that the bunched structure in the occurrence times of the second ELM may correspond to specific phases in the VLD3 signal.

Figure 4 uses three separate panels to show the VLD3 traces and ELM times for pairs of ELMs with inter-ELM times within each of the three clusters identified in Figure 1. The format is as in Figure 3. The top panel of Figure 4 shows all pairs of ELMs with inter-ELM time intervals $\Delta t < 0.015$. These are the prompt ELMs, which can all be seen to arrive after about one-and-a-half to one-and-three-quarters oscillations of the VLD3 response to the previous ELM. The centre panel of Figure 4 plots pairs of ELMs with inter-ELM time intervals $0.015 < \Delta t < 0.025$. The second ELM can be seen to occur around a specific phase of the VLD3 signal. The lower panel shows pairs of ELMs for which $\Delta t > 0.025$. Any phase relationship with the VLD3 signal is less clear than in the upper panels of Figure 4. We obtain similar results using the VLD2 signal. As can be seen from Figure 1, all of the JET plasmas in this sequence (83 769–83 775) exhibit the same structure in the statistics of their inter-ELM time intervals, including prompt ELMs which occur in a time interval $0.01 < \Delta t < 0.015$ following the previous ELM. The corresponding features, and characteristic timescales of the full flux loop signals following an ELM, shown in Figures 2–4, are seen in all of these plasmas.

## III. FULL FLUX LOOP INSTANTANEOUS PHASE

The above results suggest the existence of a link between inter-ELM time intervals and the phase of the full flux loop signals VLD2 and VLD3. Instead of inferring the phase of the full flux loop signals from visual inspection of the time series as above, we will now obtain it by direct time domain analysis of these signals, and compare it with ELM occurrence times.

An instantaneous phase can be inferred from the complex analytic signal,[14] which defines the instantaneous amplitude $A(t)$ and frequency $\omega(t)$ for a real signal $S(t)$ such that the instantaneous phase $\phi(t) = \omega(t)t$. A time series $S(t)$ has a corresponding analytic signal defined by $S(t) + iH(t) = A\exp[i\phi(t)]$, where $H(t)$ is the Hilbert transform[14–17] of $S(t)$. The full flux loop signals are sufficiently strong that we can use this method to determine their instantaneous phase. The instantaneous phase cannot be directly extracted for the Be II signal because its noise level is usually too high. In principle, differentiating the time dependent phase would yield the instantaneous frequency,[18] but here the experimental data are too noisy. To obtain the phase of the full flux loop signals, we work with 3 point spline-smoothed time series, mean-subtracted as in Figure 2, and compute the analytic signal by Hilbert transform for each inter-ELM time interval of data. The signal analyzed must oscillate about zero in order for the instantaneous phase to be well determined from the analytic signal, and we have tested that this is the case for the local mean-subtracted signals described above. The Hilbert transform requires a single-sided Fourier transform which is approximated via fast Fourier transform over the finite time window of the data. We choose an end-time for the time window to avoid edge effects.

In Figures 5(a)–5(d), we plot the instantaneous phase of the full flux loop signal versus time for all the ELMs in JET plasma 83770. We again need to choose a zero time $t_0$ from which to measure changes in the full flux loop phase following an ELM. In Figures 5(a) and 5(b), we set $t_0 = t_{ELM1}$, the time of the first ELM as determined from the Be II signal. The main figure panel plots time from $t_0$, that is, $\Delta t = t - t_0$ versus the instantaneous phase difference $\Delta\phi = \phi(t) - \phi(t_0)$ of the VLD2 (Figure 5(a)) and VLD3 (Figure 5(b)) signals. The first (red circle) and second (green circle) ELM times, as determined from the Be II signal, are overplotted on each corresponding VLD2 and 3 trace. On these plots, the first ELM always has coordinates $\Delta t = 0$ and $\Delta\phi = 0$ by definition. The coordinates of the second ELM are $\Delta t = t_{ELM2} - t_{ELM1}$ and $\Delta\phi = \phi(t_{ELM2}) - \phi(t_{ELM1})$. Histograms are shown of the $\Delta t$ (top panel) and $\Delta\phi$ (right panel) for all the ELMs. The prompt ELMs with $\Delta t < 0.015$, indicated by

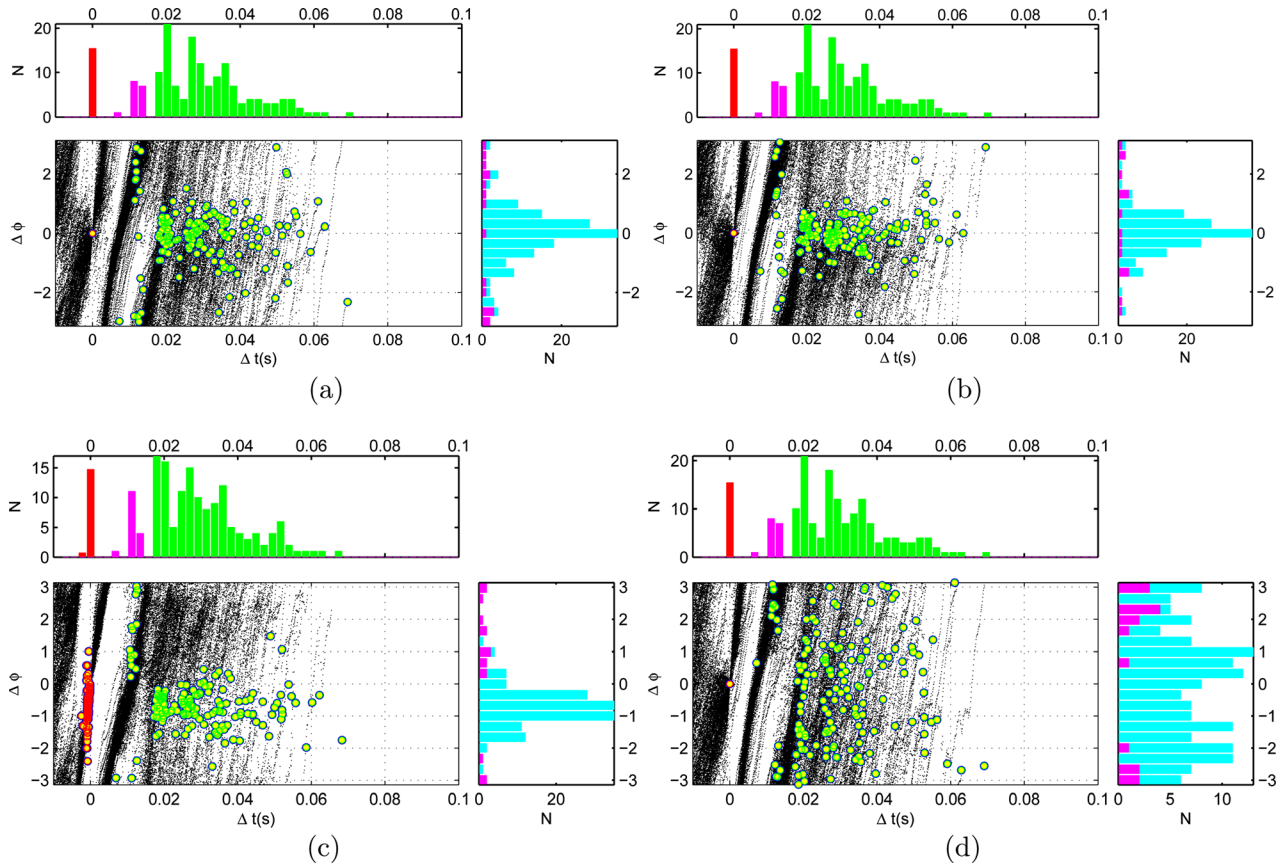


FIG. 5. ELM occurrence times and VLD phase shown for the flat-top of JET plasma 83770. The format of each set of panels is as follows: Main panel: VLD instantaneous phase, modulo $2\pi$, plotted as a function of time following each ELM up to the occurrence time of the next ELM. The coordinates are time $\Delta t = t - t_0$ and phase difference $\Delta\phi = \phi(t) - \phi(t_0)$. ELM occurrence times are marked on each VLD trace with yellow filled red circles (first ELM) and green circles (second ELM). Right hand panel: histogram of VLD $\Delta\phi$ at the time of all the second ELMs (blue), overplotted (pink) for the prompt ELMs with inter-ELM time intervals $\Delta t < 0.015$. Top Panel: histogram of ELM occurrence times $\Delta t = t - t_0$ for the first ELM (red) and the second ELMs (green), overplotted (pink) for the prompt ELMs. The frequency $N$ of first ELM times has been divided by 10. The four sets of panels show: (a) VLD2, where $t_0$ is the occurrence time of the first ELM; (b) VLD3, where $t_0$ is the occurrence time of the first ELM; (c) VLD2, now with $t_0$ at the time of the flux loop first minimum; (d) VLD2, where $t_0$ is the occurrence time of the first ELM and the time order of the inter-ELM time intervals has been randomly shuffled.

pink bars, are distinct in both arrival time and phase. All other ELMs are phase bunched with a peak around zero phase. The extrema of the large amplitude VLD2 and 3 responses to an ELM are determined more precisely in time than the ELM time from the peak in the Be II signal. In Figure 5(c), we replot Figure 5(a), but now we set $t_0$ to the first minimum in the VLD2 signal. In this plot, the phase bunching can be seen to be better defined, and the peak is shifted in phase because the phase difference is now determined over a shorter time interval.

The same phase bunching is found for *all* non-prompt ELMs in the flat-top period of H-mode in all these plasmas. The inter-ELM time intervals are not random: there is structure in the arrival time histograms. Our results show that ELMs are more likely to occur when the full flux loop signals are at a specific phase with respect to that of the preceding ELM.

We now establish that this is not be a trivial correlation. An example of a trivial correlation would be that the ELM arrival times were roughly periodic, or were at multiples of some period, and the full flux loop signals were roughly sinusoidal. In such a case, one could re-order the time sequence of the inter-ELM time intervals $\{\Delta t_1, \Delta t_2, ...\Delta t_j..\Delta t_N\}$ without changing the phase of the full flux loop signals at the ELM arrival time.

We have generated a shuffled surrogate set of ELM arrival times from the data as follows. The surrogate occurrence time of an ELM is set as $t_N = t_{N-1} + \Delta t_j$, where the inter-ELM time interval $\Delta t_j$ is now selected at random from the set of observed inter-ELM time intervals in the flat top of a given plasma. This is performed by randomly shuffling the index $j$, which preserves all the inter-ELM times. Each observed ELM pair then has a corresponding surrogate phase difference $\Delta\phi_s = \phi(t_s) - \phi(t_0)$, where $t_0$ is the arrival time of the first ELM and the second ELM has surrogate arrival time $t_s = t_0 + \Delta t_j$. The $\Delta t_j$ is drawn from the randomly permutated set of observed inter-ELM time intervals. Again, $\phi(t)$ is the instantaneous phase of the VLD2 or 3 signal determined by the same procedure discussed above. Under this operation, the histogram of ELM arrival times shown in the preceding figures is unchanged. This is shown in Figure 5(d), which is identical to Figure 5(a) except that the sequence of ELM arrival times has been replaced with our surrogate. On this plot, we see that the statistical distribution of ELM arrival times is unchanged but the phase bunching is completely lost. The phases of the surrogate data do not show a statistically

significant peak: for the histogram shown in Figure 5(d) the mean counts per bin is 7.7 giving a normal estimated ("$\sqrt{N}$") standard deviation of $\pm \sim 3$. The peak of the phase histogram in Figure 5(a) has ~30 counts per bin which is over six standard deviations away from the surrogate.

This confirms that the phase of the full flux loop signals contains information in addition to that of the statistics of inter-ELM arrival times. The phase relationship that we have found is therefore a non-trivial correlation. We have repeated the above procedure for all the other JET plasmas in this sequence, and we obtain the same results. Specifically, all of these plasmas show the same phase relationship and this is lost under the above surrogate procedure.

The above methods are only effective if the full flux loop signals have good signal/noise, do not have too large a dynamic range in response to all the ELMs, and if the mean of the signal does not vary too rapidly. In order to obtain the phase via Hilbert transform, mean subtraction is needed to centre the signal about zero over several cycles. The high rate of change of instantaneous phase with time of the full flux loop signals (see, e.g., Figure 5) requires well defined ELM occurrence times in order to cleanly determine any phase relationship.

## IV. CONCLUSIONS

We have performed a direct time domain analysis that compares the occurrence times of ELM bursts as determined from Be II emission with the instantaneous phase of the VLD2 and 3 full flux loop signals in JET. We have focused on a sequence of JET plasmas, in each of which there is a steady flat-top for $\sim 5\,s$. These all exhibit intrinsic ELMing in that there is no attempt to trigger ELMs; the only externally applied time varying fields are those required by the control system to maintain the plasma.

The full flux loop signals show a clear oscillatory response to an ELM on $\sim 0.01\,s$. We have identified a class of prompt ELMs which all occur whilst this response to the previous ELM is still at large amplitude, after about one-and-a-half to one-and-three-quarters oscillations of this full flux loop response signal. These prompt ELMs form a distinct cluster in the distribution of inter-ELM time intervals, which is almost always in the range $0.01$–$0.015\,s$. This suggests that the prompt ELMs may be directly precipitated by the large scale plasma response to the previous ELM.

A $\sim 0.01\,s$ timescale is characteristic of the integrated response time of the control system.[11] There are other aspects of tokamak engineering physics that could also give rise to effects on this timescale. These include, but are not restricted to, the timescale of variations in the sharing of total divertor coil current between the divertor coils driven by the control system, and radial motion of the plasma with associated changes in the strike point location at divertor plates.

All other, non-prompt, ELMs arrive $>0.015\,s$ after the preceding ELM, by which time the response to the previous ELM in the full flux loop signals is decaying in amplitude. We determined the difference in the instantaneous full flux loop signal phase from the time of one ELM to the next. We find that all of the non-prompt ELMs in all of these plasmas tend to occur at times when this phase difference is approximately zero: they are phase-bunched with respect to the full flux loop signals. We verified that this result is not simply a consequence of the time structure in the statistics of inter-ELM time intervals; randomly shuffling the time order of inter-ELM time intervals whilst preserving their probability distribution destroys this phase bunching.

In this paper, we have presented a novel study of the ELMing process in selected JET H-mode plasmas. Our analysis of the time evolution of simultaneous Be II emission and full flux loop VLD2 and VLD3 signals provides a fresh perspective on several aspects of this key phenomenon. This perspective combines experimental information that is essentially local to the JET edge plasma (Be II) with information reflecting the global state of the JET plasma (full flux loop). We have identified a new class of prompt ELMs, which are seen at distinct short inter-ELM time intervals. For these ELMs, the initial ELM and its successor form a linked pair, in that the second ELM arises near the end of the first, large amplitude, cycle of the full flux loop response to the first ELM. The two ELMs may be, in this sense, aspects of a single underlying plasma phenomenon. Our investigation of non-prompt ELMs, which occur at larger time separations, shows that the times at which the second ELM occurs are bunched with respect to the phase of the full flux loop signal. This may contribute towards explaining the strong statistical bunching of inter-ELM time intervals that was recently established from careful analysis of a large number of quasi-identical JET plasmas.[13] Our results for both prompt and non-prompt ELMs together suggest that deeper understanding is needed of the links between the overall ELMing process and the evolving global state of the plasma. It is not yet clear which properties of the JET tokamak plasma fix the value of the characteristic inter-ELM timescales that we have isolated. This is a complex question for further investigation together with the possibility that the full flux loop signal may contain precursor information for ELM events. We note that this knowledge may assist the design of experiments for ELM mitigation and control. It might also be of value to establish whether the ELM bunching phenomenology seen here is likely to occur in any ITER plasmas, and, if so, to determine the corresponding timescales.

## ACKNOWLEDGMENTS

We acknowledge the EPSRC and CCFE for financial support. This work, supported by the European Communities under the Contract of Association between EURATOM and CCFE, was carried out within the framework of the European Fusion Development Agreement. The views and opinions expressed herein do not necessarily reflect those of the European Commission. This work was also funded in part by the RCUK Energy Programme under Grant No. EP/I501045. This work was done under the JET-EFDA work programme. N.W.W. acknowledges the stimulating environment of the Natural Complexity Project at BAS, and J. Davidsen for discussions.

[1]M. Keilhacker, Plasma Phys. Controlled Fusion **26**, 49 (1984).
[2]V. Erckmann, F. Wagner, J. Baldzuhn, R. Brakel, R. Burhenn, U. Gasparino, P. Grigull, H. J. Hartfuss, J. V. Hofmann, R. Jaenicke *et al.* Phys. Rev. Lett. **70**, 2086 (1993).

[3]H. Zohm, Plasma Phys. Controlled Fusion **38**, 105 (1996).
[4]A. Loarte, G. Saibene, R. Sartori, D. Campbell, M. Becoulet, L. Horton, T. Eich, A. Herrmann, G. Matthews, N. Asakura, A. Chankin, A. Leonard, G. Porter, G. Federici, G. Janeschitz, M. Shimada, and M. Sugiharaet, Plasma Phys. Controlled Fusion **45**, 1549 (2003).
[5]K. Kamiya, N. Asakura, J. Boedo, T. Eich, G. Federici, M. Fenstermacher, K. Finken, A. Herrmann, J. Terry, A. Kirk, B. Koch, A. Loarte, R. Maingi, R. Maqueda, E. Nardon, N. Oyama, and R. Sartori, Plasma Phys. Controlled Fusion **49**, S43 (2007).
[6]R. J. Hawryluk, D. J. Campbell, G. Janeschitz, P. R. Thomas, R. Albanese, R. Ambrosino, C. Bachmann, L. Baylor, M. Becoulet, I. Benfatto, J. Bialek *et al.*, Nucl. Fusion **49**, 065012 (2009).
[7]G. S. Yun, W. Lee, M. J. Choi, J. Lee, H. K. Park, B. Tobias, C. W. Domier, N. C. Luhmann, Jr., A. J. H. Donn, J. H. Lee, and KSTAR Team, Phys. Rev. Lett. **107**, 045004 (2011).
[8]A. W. Degeling, Y. R. Martin, P. E. Bak, J. B. Lister, and X. Llobet, Plasma Phys. Controlled Fusion **43**, 1671 (2001).
[9]J. Greenhough, S. C. Chapman, R. O. Dendy, and D. J. Ward, Plasma Phys. Controlled Fusion **45**, 747 (2003).
[10]F. A. Calderon, R. O. Dendy, S. C. Chapman, A. J. Webster, B. Alper, R. M. Nicol, and JET EDFA Contributors, Phys. Plasmas **20**, 042306 (2013).
[11]A. Murari, E. Peluso, P. Gaudio, M. Gelfusa, F. Maviglia, N. Hawkes, and JET-EFDA Contributors, Plasma Phys. Controlled Fusion **54**, 105005 (2012).
[12]A. J. Webster and R. O. Dendy, Phys. Rev. Lett. **110**, 155004 (2013).
[13]A. Webster, R. O. Dendy, F. Calderon, S. C. Chapman, E. Delabie, D. Dodt, R. Felton, T. Todd, V. Riccardo, B. Alper, S. Brezinsek *et al.*, "Time-resonant tokamak plasma edge instabilities," Plasma Phys. Controlled Fusion (in press).
[14]R. N. Bracewell, *The Fourier Transform and Its Applications*, 2nd ed. (McGraw Hill, 1986).
[15]M. G. Rosenblum, A. S. Pikovsky, and J. Kurths, Phys. Rev. Lett. **76**, 1804 (1996).
[16]P. J. Schreier and L. L. Scharf, *Statistical Signal Processing of Complex-Valued Data* (Cambridge University Press, 2010).
[17]A. Pikovsky, M. G. Rosenblum, and J. Kurths, *Synchronization: A Universal Concept in Nonlinear Sciences* (Cambridge University Press, 2003).
[18]J. T. C. Schwabedal and A. S. Pikovsky, Phys. Rev. Lett. **110**, 204102 (2013).